Temporal Frequency of Whisker Movement. I. Representations in Brain Stem and Thalamus

RONEN SOSNIK, SEBASTIAN HAIDARLIU, AND EHUD AHISSAR
Department of Neurobiology, The Weizmann Institute of Science, Rehovot 76100, Israel

Sosnik, Ronen, Sebastian Haidarliu, and Ehud Ahissar. Temporal frequency of whisker movement. I. Representations in brain stem and thalamus. *J Neurophysiol* 86: 339–353, 2001. How does processing of information change the internal representations used in subsequent stages of sensory pathways? To approach this question, we studied the representations of whisker movements in the lemniscal and paralemniscal pathways of the rat vibrissal system. We recently suggested that these two pathways encode movement frequency in different ways. We proposed that paralemniscal thalamocortical circuits, functioning as phase-locked loops (PLLs), translate temporally coded information into a rate code. Here we focus on the two major trigeminal nuclei of the brain stem, nucleus principalis and subnucleus interpolaris, and on their thalamic targets, the ventral posteromedial nucleus (VPM) and the medial division of the posterior nucleus (POm). This is the first study in which these brain stem and thalamic nuclei were explored together in the same animals and using the same stimuli. We studied both single- and multi-unit activity. We moved the whiskers both mechanically and by air puffs; here we present air-puff-induced movements because they are more similar to natural movements than movements induced by mechanical stimulations. We describe the basic properties of the responses in these brain stem and thalamic nuclei. The responses in both brain stem nuclei were similar; responses to air puffs were mostly tonic and followed the trajectory of whisker movement. The responses in the two thalamic nuclei were similar during low-frequency stimulations or during the first pulses of high-frequency stimulations, exhibiting more phasic responses than those of brain stem neurons. However, with frequencies >2 Hz, VPM and POm responses differed, generating different representations of the stimulus frequency. In the VPM, response amplitudes (instantaneous firing rates) and spike counts (total number of spikes per stimulus cycle) decreased as a function of the frequency. In the POm, latencies increased and spike count decreased as a function of the frequency. Having described the basic response properties in the four nuclei, we then focus on a specific test of our PLL hypothesis for coding in the paralemniscal pathway. We used short-duration air puffs, much shorter than whisker movements during natural whisking. The activity in this situation was consistent with the prediction we made on the basis of the PLL hypothesis.

INTRODUCTION

The trigeminal system of rats contains two parallel anatomical pathways that extend from the vibrissae to the cortex (Diamond and Armstrong-James 1992; Woolsey 1997): the lemniscal pathway, which ascends via the ventral posteromedial thalamic nucleus (VPM), and the paralemniscal pathway, which ascends via the medial division of the posterior thalamic nucleus (POm). The two thalamic nuclei (VPM and POm) receive their main afferent input from two trigeminal nuclei in the brain stem: principal sensory trigeminal nucleus (Pr5) and interpolar part of the spinal trigeminal nucleus (Sp5I) (Bruce et al. 1987; Erzurumlu and Killackey 1980; Peschanski 1984; Veinante et al. 2000). Although both these brain stem nuclei project to both of the thalamic nuclei, the primary input to the VPM arrives from Pr5, whereas that of the POm arrives from Sp5I (Chiaia et al. 1991a; Friedberg et al. 1999; Rhoades et al. 1987; Williams et al. 1994). The lemniscal pathway contains large-diameter axons that end in focal, clustered terminals (Bishop 1959; Chiaia et al. 1991a; Williams et al. 1994). Lemniscal neurons respond with short, constant latencies (Ahissar et al. 2000; Diamond et al. 1992) and have relatively small receptive field (RF) centers under deep anesthesia (Diamond et al. 1992; Friedberg et al. 1999). The paralemniscal pathway contains axons with smaller diameters than those of the lemniscal pathway and form more diffuse connections (Bishop 1959; Chiaia et al. 1991a; Veinante et al. 2000; Williams et al. 1994). Paralemniscal neurons exhibit slower responses, longer and more variable latencies (Ahissar et al. 2000; Diamond et al. 1992), and larger RF centers during deep anesthesia than lemniscal ones (Diamond et al. 1992). Interestingly, the size of the entire RF, including weak inputs, does not differ significantly between the two nuclei (Diamond et al. 1992; Friedberg et al. 1999; Nicolelis and Chapin 1994).

The significance of brain-stem-to-thalamus transformations was not fully appreciated previously because brain stem and thalamic responses had not been compared for identical stimuli. Furthermore, most studies used stimuli designed to explore basic features of brain stem and thalamic responses, such as RF size, directional selectivity, and velocity thresholds (Armstrong-James and Callahan 1991; Chiaia et al. 1991b; Diamond et al. 1992; Nicolelis et al. 1993; Shipley 1974; Simons and Carvell 1989; Waite 1973) and thus did not resemble the stimuli generated by natural activation of whiskers during whisking. On the other hand, when neurons are recorded during self-initiated whisker movements in the awake rat, experimental control of the whisker movement is limited (Nicolelis and Chapin 1994; Nicolelis et al. 1995). With experiments in anesthetized and awake animals, Nicolelis and colleagues demonstrated that the VPM nucleus does not function as a simple relay but rather probably participates in spatial processing of vibrissal information (Ghazanfar and Nicolelis 1997; Ghazanfar et al. 2000; Nicolelis and Chapin 1994) (by spatial processing we mean computation based on the spatial configuration of

Address reprint requests to E. Ahissar (E-mail: Ehud.Ahissar@weizmann.ac.il).

the activated whiskers). These findings, together with reports of higher spatial resolution in lemniscal than paralemniscal stations (Armstrong-James and Fox 1987; Diamond 1995; Simons 1995), suggest that the *lemniscal system processes spatially encoded information*. Our recent findings support this notion and further suggest that the *paralemniscal pathway processes temporally encoded information* (Ahissar et al. 2000). The paralemniscal system represents temporal information by both the latency and spike count of thalamic and cortical neurons. These representations were previously predicted by our phase-locked loop (PLL) hypothesis (Ahissar 1998; Ahissar and Vaadia 1990; Ahissar et al. 1997). We use the term "representation" here to refer to a neuronal variable that changes as a function of a stimulus quantity in such a manner that the quantity can be reconstructed from the variable. According to the PLL hypothesis, the spike-count representation is the output of the thalamocortical circuits and is used for further cortical processing, whereas the latency representation is an internal variable of the decoding process.

The findings described in the preceding text indicate that significant transformations occur already between the brain stem and the thalamus. Here, we investigated the characteristics of the transformation from the brain stem to the thalamic nuclei of both pathways in the anesthetized rat during constant-frequency tactile stimulations. Two types of tactile stimuli (air puffs to groups of whiskers and mechanical deflections of single whiskers) and two pulse widths (50 and 20 ms) were applied. The representation of a single stimulus pulse was different for air-puff and mechanical stimulations but was similar in both thalamic nuclei; i.e., a single stimulation, of either method, evoked similar responses in both VPM and POm. In contrast, the representation of the stimulus frequency was different in the two thalamic nuclei. The only consistent thalamic representation of the stimulation frequency was the spike count of POm neurons. This latter finding, which is consistent with our PLL hypothesis, suggests that the POm spike-count codes whisker frequency for cortical processing.

METHODS

Animal procedures and electrophysiology

Experimental procedures were similar to those previously described (Ahissar et al. 1997; Haidarliu and Ahissar 1997). Briefly, 30 adult male Wistar Albino rats (300 $\pm$ 25 g; obtained from the Animal Breeding Unit of The Weizmann Institute of Science) were anesthetized (urethan, 1.5 g/kg ip) and mounted in a modified stereotaxic device (Haidarliu 1996) that allows free access to the somatosensory brain structures and to the vibrissae. The depth of anesthesia was monitored by assessing corneal reflex and was maintained at stage III/3–4 (Friedberg et al. 1999) by supplementary injections of urethan (10% of initial dose). Atropine methyl nitrate (0.3 mg/kg im) was administered before general anesthesia to prevent respiratory complications. Body temperature was maintained at ~37°C. The skull was exposed, and openings were made to allow for electrode penetrations into different nuclei in the thalamus and brain stem. The procedures for electrode penetrations into these nuclei were described in detail elsewhere (Haidarliu et al. 1999). Briefly, for thalamic penetrations, the electrodes were directed vertically, touching dura between 3.5 and 4.3 mm caudal to Bregma and 1.6 and 3.0 mm laterally from midline. For brain stem penetrations, the electrodes were directed obliquely, touching dura between 6 and 8 mm caudal to Bregma, and from 1.5 to 3.5 mm laterally, ipsilateral to the stimulated whiskers; the electrodes were inserted with an angle of ~50° to penetrate into Pr5 and 40° to penetrate into Sp5I. Four or eight microelectrodes were simul-

taneously driven into one, two, or three nuclei using one or two microdrive systems (Haidarliu et al. 1999). Single units were isolated by spike templates and multi-units by amplitudes using spike sorters (MSD-2; Alpha-Omega) (Haidarliu et al. 1995). The experimentation was conducted in conformity with the Guiding Principles for Research Involving Animals and Human Beings, and with the animal welfare guidelines of The Weizmann Institute of Science.

Whisker stimulation

Whiskers were stimulated by either air puffs or mechanical deflections. Air puffs consisted of pulses of compressed air, which were generated by a pneumatic pressure pump (Medical Systems; Greenvale, NY) and were delivered via a 3-m length of stiff, thick-walled tubing (6.5 mm OD, 3.5 mm ID). A micropipetter tip was attached to the end of the tubing to reduce its opening to a diameter of 0.7 mm and was positioned 10–20 mm caudal to the most caudal whiskers of the stimulated rows. Before positioning the air-puff stimulator, the RFs of all simultaneously recorded neurons were determined; the RFs were defined as those whiskers whose deflection could elicit a noticeable response in the neuronal activity as judged by listening to the acoustic conversion of the amplified electrode signal. One to three rows of whiskers, which contained the entire RF of most of the simultaneously recorded neurons, were stimulated; at least four whiskers were stimulated in each row. The neurons whose RFs were not stimulated were excluded from analysis. The analog voltage, which represents the output pressure of the pump, was continuously monitored and recorded (see Figs. 1, 2, and 8). The maximum pressure at the pump output was 0.7 kg/cm^2. Air-puff delays (from pump command to whisker movement) were calibrated using a microphone. Mechanical stimuli were generated by a linear electromagnetic vibrator (Schneider 1988) that was attached to a single (the "principal") whisker (Haidarliu et al. 1999). The position and movement profile of the vibrator was determined by a built-in photodiode whose output voltage was continuously monitored and recorded (see Fig. 1). Both air-puff and mechanical stimuli were applied in the protraction direction. For each recording, latencies evoked by air puffs were adjusted by comparing the latencies to the first stimulus cycles at 2 or 5 Hz with those evoked by the mechanical stimulator; if a difference was detected, it was subtracted from all air-puff latencies of that recording. The movement profile of the whiskers during air-puff stimulations was examined in two rats using a motion scope (PCI 1000, Red Lake). The position of a single spot on a single whisker, at a distance of 5 mm from the face, was tracked at a resolution of 2 ms at all frequencies and pulse widths. Movement profiles (see Fig. 1) were constant along the trains and for all frequencies.

Stimuli were applied in blocks, each containing several trains (trials) of identical parameters. Two types of frequency patterns and two widths of stimulus pulses were applied. Trains of constant frequencies were applied in blocks of 12 consecutive trains of 3 or 4 s with inter-train intervals of 2 or 1 s, respectively. The order of the blocks was usually as follows: 2, 5, 8, 11, (sometimes 14), (45-s interval), (sometimes 14), 11, 8, 5, and 2 Hz, with inter-block intervals of 10 s (data for the 14-Hz stimuli, which usually evoked weak thalamic responses, are not presented; in a few cases only 2, 5, and 8 Hz were applied). Thus for each frequency a total of 24 trains were applied. Data from all 24 trains were used to compute average latencies and spike counts (see *Data analysis*). During the initial phase of the study, the order of the frequency blocks was randomized. No qualitative or quantitative differences between the different orders was observed. Each set of constant frequency blocks was applied with the same pulse width, 20 or 50 ms.

Histology

The brains of the rats were examined histologically to determine the location of each and every recording site. At the end of each recording session, electrolytic lesions were induced by passing currents (3–5 μA, 2 $\times$ 2 s, unipolar) through the tips of the electrodes. When

multiple recording sites were obtained with the same electrode, the electrode was re-positioned at each depth that corresponded to a previous recording site (provided that it was >200 μm away from the previous lesion), and lesion currents were passed in those locations as well. Each rat was then killed with Pental (pentobarbitone 200 mg/ml; 0.5 ml pro capito, ip), and perfused transcardially with 2.5% glutaraldehyde, 0.5% paraformaldehyde, and 5% sucrose in 0.1 M phosphate buffer, pH 7.4. The brains were removed, sectioned coronally, and stained for cytochrome oxidase activity (Haidarliu and Ahissar 1997). In these preparations, the different nuclei of the thalamus and brain stem, the lesions, and the tracks of the electrodes were clearly seen (Haidarliu and Ahissar 2001; Haidarliu et al. 1999). VPM recording sites could be affiliated with single barreloids by comparing the recording site with a three-dimensional scheme of the VPM obtained with oblique cutting angles (Haidarliu and Ahissar 2001).

Data analysis

Only data from well-localized recording sites (see Fig. 2) are described here. From each electrode tip, we recorded the activity of one, two, or, rarely, three isolated units ("single-units") as well as one or two clusters of unsorted units ("multi-units"). We assume that most of the recorded units were located within a radius of 50 μm around the electrode tip (Abeles 1975, 1982; Ahissar, unpublished observations). The location of the electrode tip was assumed to be at the center of the lesion performed at that recording site. The location of recording sites in which no lesion was performed was estimated according to the electrode track, the location of a neighboring lesion, and the corresponding penetration distances. Data were analyzed for single units, multi-units, "local populations," and "nucleus ensembles." Local populations included all single and multi-units recorded from a single electrode at a given site. The number of neurons included in a local population was estimated as 5 ± 1.3 neurons (mean ± SD, n = 48). This estimation was based on a sample of 48 local populations in which, in addition to the single units isolated by the MSD, individual spike shapes could be isolated by visual inspection of the multi-unit clusters recorded from the same electrode. Nucleus ensembles consisted of all local populations of the data set that were recorded from the same nucleus (see Georgopoulos et al. 1993 for a similar approach). Peristimulus time histograms (PSTHs) were computed using 1-ms bins and were smoothed by convolution with a right-angle triangle of area 1 and different base lengths. Unless otherwise mentioned, the base was 0–16 ms for PSTHs that accompany raster displays, and 0–8 ms for all other PSTHs.

We repeated the analysis while using alternative methods for estimating the latency of the responses. Estimations based on the latency to first spike (e.g., Diamond et al. 1992) were strongly affected by the average firing rates (see DISCUSSION). Estimations based on statistical measures of the prestimulus background activity (e.g., Petersen and Diamond 2000; Raiguel et al. 1999) were in general in agreement with the amplitude-based latency estimation (see following text) but since, during high-frequency stimulations (8 and 11 Hz), durations of background activity within the trains were often very short, statistical estimations were not reliable. Thus we prefer to present the results as analyzed by straight-forward amplitude-based estimation. Neuronal latencies were estimated from the smoothed (0–8 ms) PSTHs as the time in which the firing rate crossed a certain threshold, which was determined as a given fraction of the peak (minus background) value of the PSTH computed for that particular response and that particular stimulus cycle; thus PSTHs were computed for each stimulus cycle, and latencies were derived from each such PSTH according to its own peak value. For each analysis, latencies were computed using thresholds of 0.1, 0.3, and 0.5 of peak value (after subtracting mean background activity). All these thresholds yielded basically the same results; the basic differences between latencies in VPM and POm were evident for all these thresholds. Trial-by-trial variabilities of the latency (represented by the error bars in Figs. 3 and 6) are of the latency to the first spike after stimulus onset. Spike counts represent the average sum (per stimulus cycle) of spikes during a time window immediately after stimulus onset (80 ms, unless otherwise mentioned). All the averaged data (firing rates in PSTHs, latencies, and spike counts) presented along the stimulus train time were smoothed for presentation by a convolution with a right-angle triangle of area 1 and base of 2 stimulus cycles. Nucleus ensemble data were analyzed by averaging PSTHs, latencies, and spike counts across the local populations that composed the ensemble and by first summing all spikes of the ensemble and then computing the PSTHs, latencies, and spike counts from the ensemble spike train. Both methods yielded similar results.

RESULTS

In this study, a total of 308 single units and 221 multi-units were recorded from 160 recording sites. Of these, 146 single units and 124 multi-units were recorded from sites that could be clearly assigned to the following nuclei: 25 single units and 14 multi-units from the Pr5, 26 and 31, respectively, from the Sp5I, 45 and 42, respectively, from the VPM, and 50 and 37, respectively, from the POm. The remaining units were recorded from nuclei that are not described here (oral and caudal parts of the spinal trigeminal nucleus), from the borders between nuclei, or from sites that could not be reliably reconstructed.

Comparison of air-puff and mechanical stimulations

The movement profiles of the whiskers, induced by these two types of stimuli, are depicted in Fig. 1 (*2 bottom traces*). The mechanical stimulator was firmly attached to the whisker, and thus its movement profile was the same as that of the whisker (*right*). Whisker movements during air-puff stimulations were measured using a motion scope (*left*). Vibrissal stimulation by air puffs and mechanical vibrators differed in several ways: air puffs were applied to clusters of whiskers, whereas mechanical stimuli were applied to single (principal) whiskers; mechanical stimuli induced shorter rise and fall times than air puffs (4.5 and 4.7 vs. 30 and 22 ms, respectively; 10–90% of peak value; note that the initial rising phase of the air puff was faster than the later phase); mechanical stimuli forced both forward and backward movements, whereas air puffs forced only forward movement, which allowed self-retraction of the whiskers; and mechanical stimuli had overshooting components in both directions, whereas air puffs had none.

Average neuronal responses to these two types of stimuli were compared by pooling data from all well-localized local populations, i.e., those recorded from sites that could be clearly affiliated with a specific nucleus, which were stimulated with both stimulators and with pulse widths of 50 ms. The mean responses to the first stimulus pulse during 2-Hz stimulations are depicted in Fig. 1. Whereas air puffs evoked tonic responses along the stimulus pulse, responses to mechanical stimuli were bi-phasic, i.e., brain stem and thalamic neurons responded to both protraction and retraction. The OFF response to the mechanical deflection was clearly a response to the falling edge (backward movement) and not to the overshooting component as seen from the timing of the activity. The phasic responses of the brain stem to mechanical stimuli were preserved at the thalamus, whereas the tonic responses of the brain stem to air puffs were transformed to more phasic responses at the thalamus. The difference between the brain stem responses to the two stimulation types is critical and should be taken into account when studying internal representations of the stimulus frequency. Since with mechanical stimuli two response bursts were generated for each stimulus pulse, the actual frequency of the afferent activity from brain stem to thalamus was doubled. This
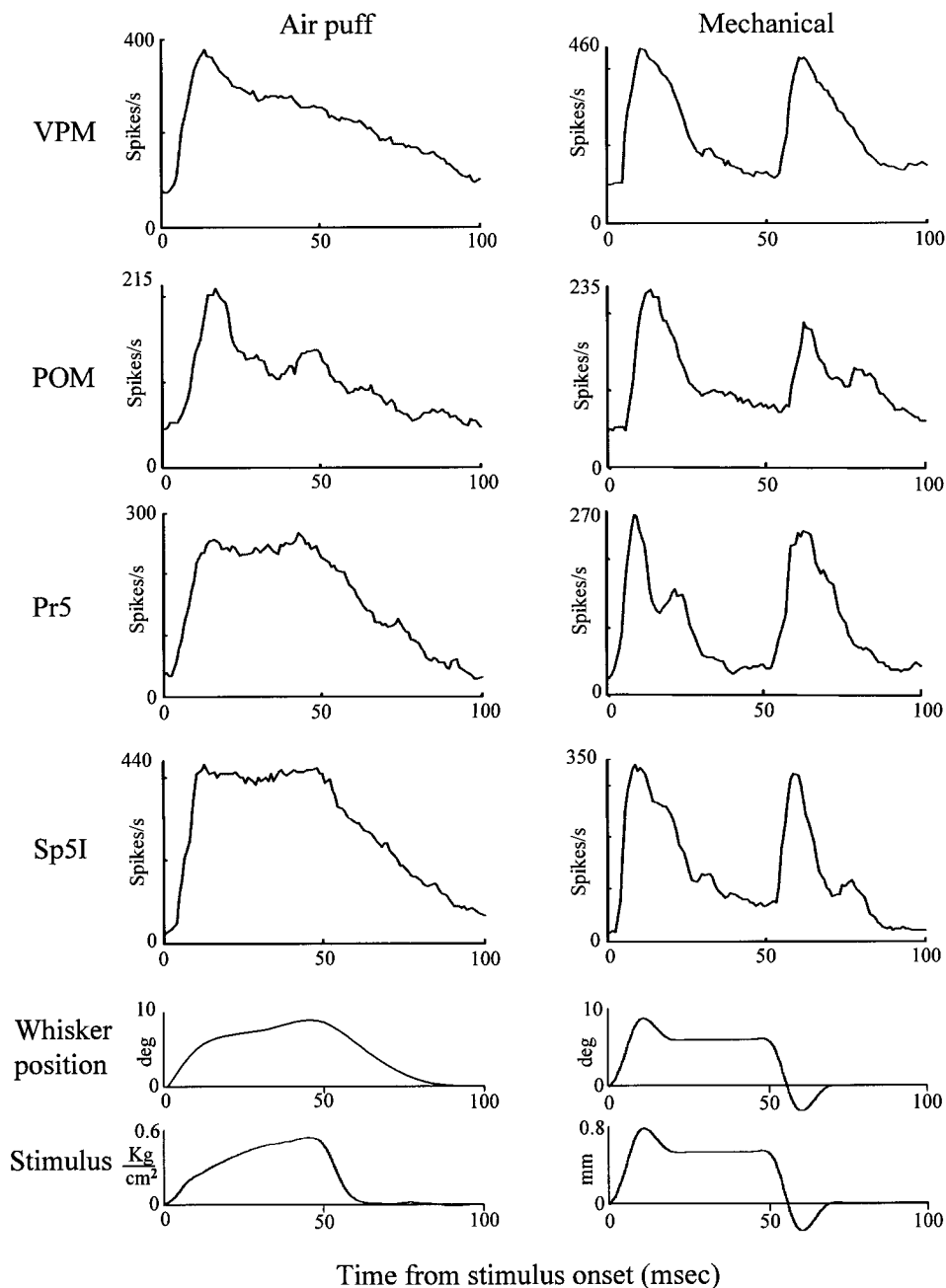
FIG. 1. Comparison of responses of local populations to air-puff and mechanical stimulation. Responses to the first cycle of the 2-Hz stimulus trains were pooled for all local neuronal populations that were stimulated with both stimulators with pulse widths 50 ms at 2 Hz in the ventral posteromedial nucleus (VPM, $n = 6$), medial division of the posterior nucleus (POm, $n = 4$), principal sensory trigeminal nucleus (Pr5, $n = 4$), and interpolar part of the spinal trigeminal nucleus (Sp5I, $n = 5$). The air-puff stimulus pattern was recorded from the analog measure of the output pressure. Whisker position during air-puff stimulation was captured with a motion scope and digitized at 2-ms resolution; traces of first and last stimulus cycles at all frequencies were averaged and low-pass filtered (2 poles) at 100 Hz. The delay between the air-puff stimulus and the whisker movement (28 ms) is not shown. The mechanical stimulator was attached to the whisker at 5 mm from the skin and its deflections were recorded from the photodiode signal (see METHODS).

contrasts the response pattern during self-generated whisker movements in freely moving rats, where brain stem populations generate a single burst for each cycle of whisker movement (Nicolelis et al. 1995). Our air-puff stimulations, however, induced whisker movements that resembled the movement profile observed during natural whisking (compare the whisker trajectory in Fig. 1 to single protraction cycles in Fig. 4 of Carvell and Simons 1990), and evoked brain stem responses that resembled those observed in freely moving rats (Nicolelis et al. 1995). Thus the neuronal representations of the stimulus frequency were investigated here primarily using air-puff stimuli.

Typical responses to trains of air puffs

Air-puff stimulations consisted of trains of 3 or 4 s with inter-train intervals of 2 or 1 s, respectively. Typically, brain stem neurons exhibited a constant response pattern throughout the train, while thalamic neurons exhibited dynamic patterns. Typical responses at 8 Hz are depicted in Fig. 2. The responses are described by rasters of 12 consecutive trains and the PSTHs summing the responses to the 12 trains. It can be seen that in the brain stem the response to the first stimulus pulse (cycle) was similar to the responses to the subsequent pulses. However, this was not the case in the thalamus. The response of the VPM multi-unit was modulated during the first few cycles until it stabilized on a constant, steady-state response that had the same latency as the response to the first stimulus cycle but a lower amplitude. The POm multi-unit also exhibited a stabilization process, but this included a shift of the response latency to longer latencies.

Comparison of VPM and POm responses

The main difference observed between the responses of the two thalamic nuclei was in the temporal domain. VPM neurons
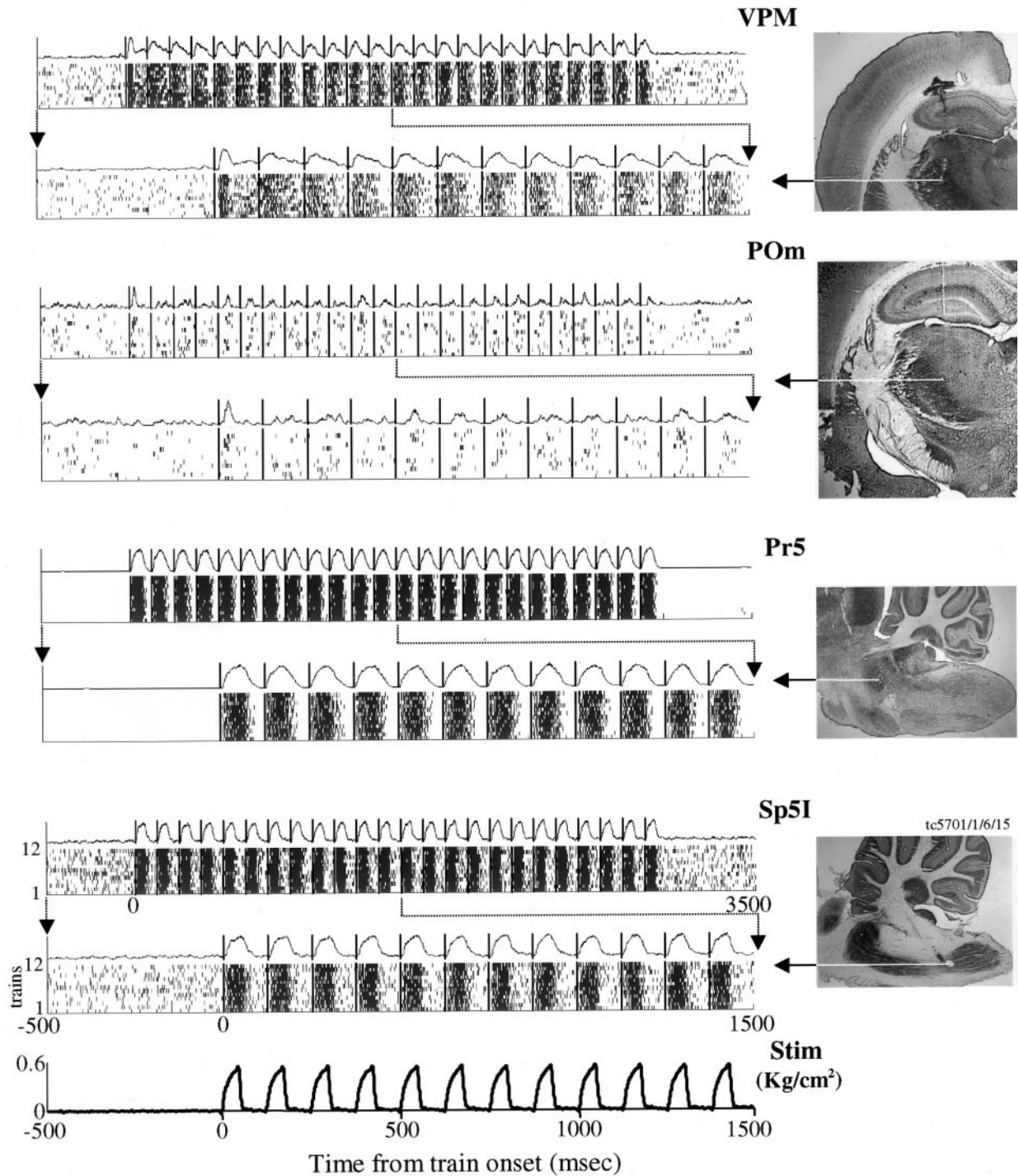
FIG. 2.   Raster displays of typical multi-unit responses in the brain stem and thalamus. Rasters for the entire stimulus train (*top row* in each panel) and for the 1st 1,500 ms (*bottom row*) are presented. Each small vertical line represents a single spike, and each long vertical line represents the onset of a single air-puff pulse. One block of 12 trains, of 3 s each, of 50-ms air-puff pulses at 8 Hz are depicted for each recording. The curves *above* the rasters are the peristimulus time histograms (PSTHs), which describe the average responses along the train. The recording sites of these units (origins of arrows) are shown on the coronal and parasagittal sections through the thalamus and brain stem, respectively, which were stained for cytochrome oxidase (*right*). Receptive fields (RFs): VPM, A1, A2; POm, C1, C2, C3, B2, B3; Pr5, D2, D3; Sp5I, D2, D3. The *bottom trace* depicts the output pressure of the pneumatic pump.

responded with a fixed latency across varying stimulus frequencies, while the latencies of POm neurons were modulated during the dynamic period until they stabilized at longer latencies during the steady-state period. We quantified these dynamics for four different stimulus frequencies: 2, 5, 8, and 11 Hz. For all four frequencies, the pulse width and train duration were the same. The only differences between the trains of different frequencies were the inter-pulse intervals and the number of pulses per train. The effect of the stimulus frequency on the steady-state response pattern was different for the two nuclei as demonstrated by the simultaneous recording depicted in Fig. 3. While the steady-state latencies of the VPM
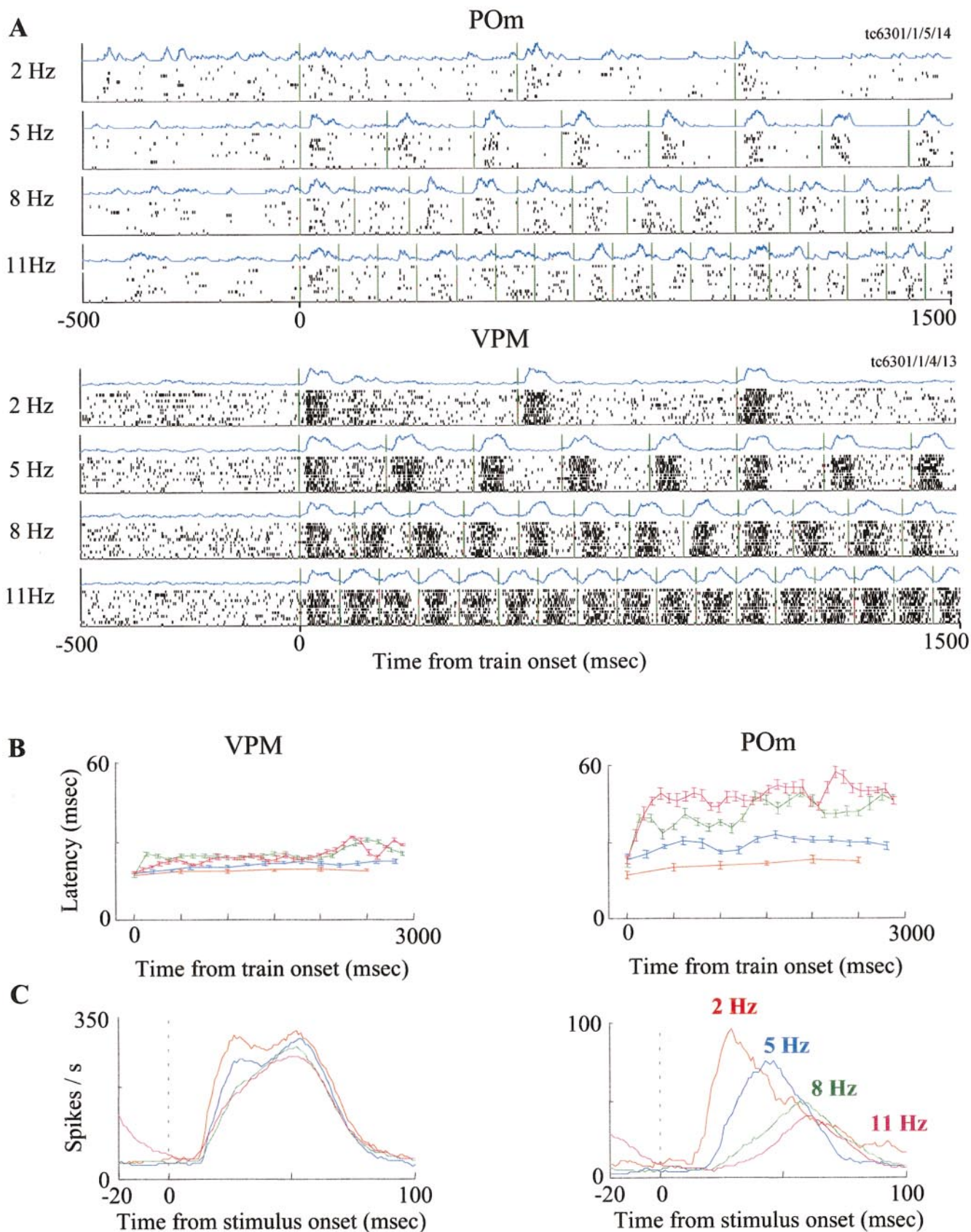
FIG. 3. Comparison of multi-unit recordings obtained simultaneously from the POm and VPM. *A*: raster displays and PSTHs for the 1st 1,500 ms of the stimulus trains at various frequencies. RFs: VPM, C1; POm, gamma, C1, C2, delta, D1. *B*: dynamics of response latency. The latency to 0.5 peak value was computed and plotted for each stimulus cycle. Standard errors of the latency were computed from the inter-train variability ($n = 24$ trains) of the latency to the 1st spike (for each stimulus cycle). Time constants of single-exponential best fits for the latencies of the POm unit were: 770, 743, 117, and 280 ms for 2, 5, 8, and 11 Hz, respectively. *C*: steady-state PSTHs for each stimulus frequency. The steady-state PSTHs were averaged across all stimulus pulses between 0.5 and 3 s from train onset.

neurons were constant for all frequencies, those of the POm neurons increased with increasing stimulus frequencies (Fig. 3, *A* and *B*). In both nuclei, the dynamic process was predominantly restricted to the first few hundred milliseconds of the train. This time period usually included between one and about six stimulus cycles, depending on the stimulus frequency. Following this period, the response amplitude and latency generally stabilized, with this steady-state period lasting until the end of the train (Fig. 3*B*). In this report, steady-state periods refer to the periods from 0.5 s after train onset until the end of the train.

The basic response differences between VPM and POm during steady states are depicted by PSTHs computed for the steady-state periods (Fig. 3*C*). Whereas in the VPM the onset latency was roughly constant, in the POm onset latencies increased with increasing frequencies; since POm offset latencies did not change, the response area decreased with the frequency.

Population analysis of steady-state responses

The steady-state responses of all well-localized local populations, are depicted in Fig. 4*A*. Although the response parameters of different local populations varied, the following observations were valid for almost all recordings. Well-localized brain stem recordings yielded a constant, nonadapting response to each single stimulus pulse. In contrast, virtually all thalamic recordings exhibited transformed responses: as the stimulus frequency increased, VPM local populations showed amplitude reduction, whereas POm neurons showed increased latencies: With all POm populations but one, onset latency increased with increasing frequencies, whereas onset latency was constant for all VPM populations. Both amplitude reductions and increased latencies resulted in reduced spike counts due to the reduction in PSTH areas. Thus stimulus frequency was represented in the VPM by amplitude reductions, in the POm by latency increments, and in both nuclei by spike-count reductions.

Figure 4 also depicts the variability in response patterns within each thalamic nucleus. Some local VPM populations exhibited amplitude reduction as a function of frequency and some not. Of those displaying amplitude reduction, some exhibited a uniform reduction along the entire response pulse while in others the reduction was mainly restricted to the early response component. However, in all 23 local populations of the VPM, there was a response component of short (and constant) latency at all frequencies. In contrast, in 17/18 local populations of the POm there were at least two frequencies at which the response commenced significantly later than the response at 2 Hz.

Single-unit responses exhibited larger variability than that depicted by the multi-unit and local population responses. However, in each nucleus, the majority of the single units exhibited the same dynamics and the same dependence on the stimulus frequency as the corresponding multi-units and local populations (see examples in Fig. 4*B*): most of POm neurons (77%) exhibited increased onset latency with increasing frequencies, whereas onset latency was constant for the majority of VPM neurons (86%). Most of brain stem neurons (77%) exhibited constant response pattern for all frequencies.
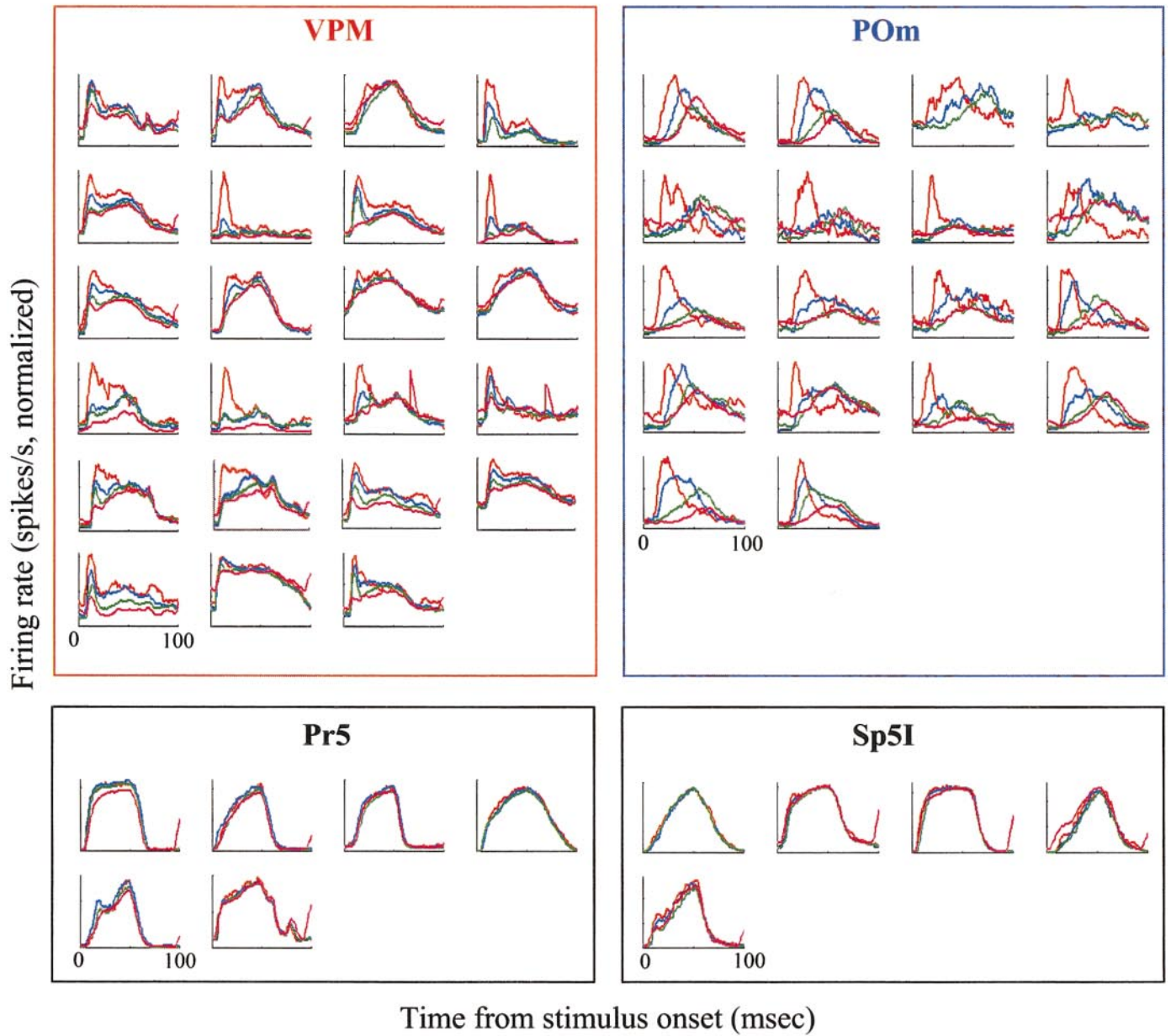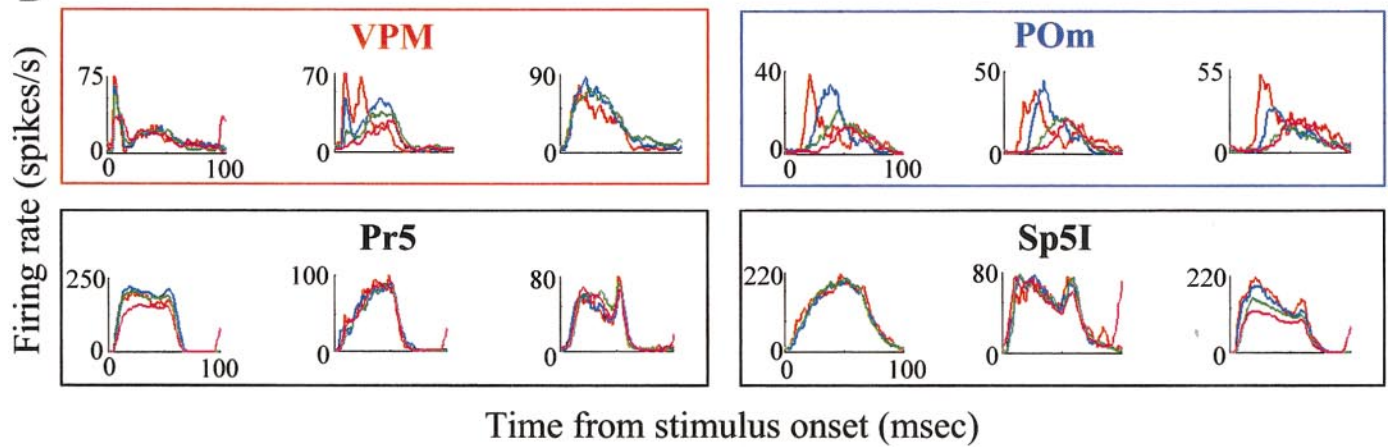
Onset latencies of neuronal populations are dominated by the onset latencies of the fastest responses within the population. To evaluate the overall latency distributions in each nucleus, PSTHs and latencies of all well-localized single and multi-units were computed (Fig. 5). The ensembles of normalized PSTHs during steady state (i.e., the period between 0.5 s after train onset until the end of the train; *left*) demonstrate the

main difference between the two thalamic nuclei: while VPM responses had a constant onset latency, onset latencies in the POm increased with the frequency. The distributions of onset latencies (to 0.5 peak value, *right*) show a frequency-invariant mode ~10 ms for VPM neurons, but frequency-dependent modes, increasing from 15 to 45 ms for POm neurons. The distributions of latencies to 0.1 and 0.3 of peak value showed similar patterns; VPM latency modes were constant ~10 ms, whereas POm modes increased from 10 to 35 and from 15 to 40 ms, respectively (data not shown). The distributions of latencies obtained with nonsmoothed PSTHs were not significantly different from those obtained with smoothed PSTHs ($P > 0.05$, 2-tailed t-test, for all nuclei and frequencies). While the dispersion of POm latencies remained more or less unchanged, that of VPM latencies increased at 11 Hz mainly due to strong attenuation of the early response component (Fig. 4). The median latencies were 9, 9, 10, and 16 ms in the VPM, and 17, 24, 36, and 43 ms in the POm, for 2, 5, 8, and 11 Hz, respectively. The latencies of POm units increased significantly for each increment of the stimulus frequency ($P < 0.01$, 1-tailed t-test, for 2 to 5, 5 to 8, and 8 to 11 Hz increments), whereas those of the VPM units did not change ($P > 0.2$, 2-tailed t-test, for all increments). POm latencies were significantly longer than those of VPM for all frequencies ($P < 1E - 8$, 2-tailed t-test). The latencies of VPM and POm units were most distinct at 8 Hz: [mean(POm latencies) – mean(VPM latencies)]/$\sqrt{}$[std(POm latencies) * std(VPM latencies)] = 1.8, 2.6, 3.3, 2.3 for 2, 5, 8 and 11 Hz, respectively, where std is the standard deviation.

Figures 4 and 5 demonstrate that, with few exceptions in each nucleus, the common response modes differed significantly between VPM and POm. This is evident from the gross ensemble representations generated by the summed activity of all well-localized neurons in each nucleus (Fig. 6*A*). These representations suggest that a typical ensemble representation, generated by the integrated activity of tens or hundreds of neurons, should exhibit an amplitude coding at the VPM and a latency coding at the POm. Although the "coding ranges" (i.e., the frequency ranges within which the latency and spike counts changed monotonically with the stimulus frequency) of individual thalamic representations did not cover the entire frequency range of 2–11 Hz and varied among different recordings (Fig. 4), the gross ensembles exhibited coding ranges that covered the entire frequency range (Fig. 6*A*).

Figure 6*A* also demonstrates the robustness of the thalamic latency coding. We define onset latencies here as the time it takes the response to cross a certain threshold (see METHODS). Since the rising edge of the PSTHs has a finite slope, latencies defined according to different threshold levels would be somewhat different. However, these differences do not change the general coding scheme. For all threshold levels between 0.1 and 0.5 peak value (*bottom* and *top blue curves,* respectively, in Fig. 6*A*), VPM neurons exhibited virtually identical latencies, whereas POm neurons exhibited significant shifts. The increased VPM latencies to 0.5 peak value at 11 Hz (Fig. 6*A*, *top blue curve*) was the result of the discrepancy between the attenuation of early and late response components of a few local VPM populations in which the early responses were reduced to <0.5 of the peak of the late responses (see Figs. 4 and 5).

With increasing frequencies, the discharge of POm neurons changed in two ways. First, the discharge latency increased; second, the overall amplitude of the discharge decreased. The

A

Firing rate (spikes/s, normalized)

VPM   POm

Pr5   Sp5I

Time from stimulus onset (msec)

B

Firing rate (spikes/s)

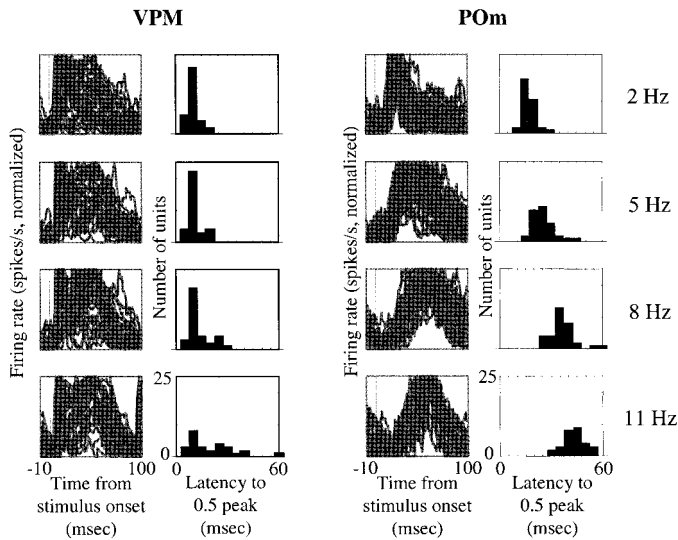VPM   POm

Pr5   Sp5I

Time from stimulus onset (msec)

FIG. 5. Response latencies of all well-localized neurons. All well-localized and responding single and multi-units of the VPM ($n = 33$) and POm ($n = 33$) are included. The steady-state PSTHs for 2, 5, 8, and 11 Hz were normalized by their maximal values (*left*). *Right*: distributions of latencies to 0.5 of peak value.

reduced amplitude of the response probably reflects the effect of increased latency on the phasic response of POm neurons (Fig. 1). Indeed, the time course of the responses to the 5-, 8-, and 11-Hz stimuli is nearly identical after ∼60 ms, consistent with the effect of a multiplicative gating mechanism (i.e., a mechanism that "gates out" the initial response component) rather than a passive delay.

Latency increments in the POm were observed both as a function of train time and as a function of frequency with the latter occurring during the steady-state periods. The dynamics of latency changes, along the entire stimulus train, for the data pooled from all well-localized recording sites, are depicted in Fig. 6B. Latency was constant for all nuclei except the POm. In the POm, latencies to the first stimulus cycles were similar for all frequencies; however, these latencies increased during the first 500–1,000 ms of the train, stabilizing at higher values for higher frequencies. The dynamics of latencies to 0.1 or 0.5 of peak value (not shown) were similar to the dynamics of the latency to 0.3 peak value (Fig. 6B), although the absolute values were slightly lower or higher, respectively.

Effect of the stimulus pulse width on the latency and spike-count representations

Figures 2–6 were obtained by using air puffs with a constant pulse width of 50 ms, which is close to the duration of the natural protraction period (Carvell and Simons 1990; Welker 1964). Whether the spike count and latency codings depend on the pulse width was tested by studying the differences between responses to air-puff pulses of 20 and 50 ms. The air-puff pulses were truncated at 20 ms without compensating for the loss of amplitude. This induced shorter whisker movements, simulating cases in which whisking cycles are shortened but the velocity is not

changed. The effect of reducing the stimulus pulse width is demonstrated in Fig. 7, showing the nuclei ensemble representations generated by the summed activity of all well-localized neurons in each nucleus that were tested with both pulse widths.

The responses of the brain stem neurons to the 20-ms pulses were similar to a truncation at 20 ms of their responses to 50-ms pulses (Fig. 7, Pr5 and Sp5I). Consequently, the latency and spike count remained essentially independent of the stimulus frequency. In contrast with brain stem responses, reduction of the stimulus pulse width led to marked reductions in amplitude coding in VPM and in latency coding in POm (see PSTHs in Fig. 7). Amplitude equalization in the VPM resulted in the spike-count coding almost disappearing; with 20-ms pulses, spike counts for all frequencies were nearly equal (Fig. 7, tuning curves). In the POm, latencies were still increasing as a function of frequency, but to a much lesser degree than with 50-ms pulses. This reduction in POm latency coding resulted in preservation of the spike-count coding such that it was similar to that obtained with 50-ms pulse widths. This occurred because the reduction in onset latency followed the reduction in pulse width, which together resulted in almost no change in spike counts (Fig. 7; see areas under the PSTHs and tuning curves). Thus the reduction of the stimulus pulse width resulted in reduced spike counts in both brain stem nuclei and in inverted effects in the two thalamic nuclei: reduction of spike-count coding with no latency change in the VPM and reduction of latency coding with no spike-count change in the POm.

The effect of the stimulus pulse width on the thalamic representations is summarized in Fig. 8. The reduction of the pulse width from 50 to 20 ms significantly affected the spike-count representation in the VPM (2-way ANOVA, $P = 0.007$) and the latency representation in the POm (2-way ANOVA, $P < 1E - 7$). However, neither the latency representation in the VPM nor the spike-count representation in the POm were changed (2-way ANOVA, $P > 0.5$ for both). Thus fixed latency is preserved in the lemniscal system and invariant spike-count coding is preserved in the paralemniscal system, while VPM spike counts and POm latencies change when the pulse width changes.

The dependence of thalamic representations on the pulse width might suggest that these representations depend primarily on the inter-stimulus interval (ISI), i.e., the interval between the end of the stimulus pulse and the beginning of the next pulse, rather than on the frequency per se. The dependence of the latency and spike-count representations on the ISI was tested with the data that was obtained with both pulse widths. Whereas POm spike counts usually increased with increasing ISIs, neither the VPM spike-count representation nor the POm latency representation displayed consistent behavior as a function of the ISI. In fact, with different frequencies and pulse widths, similar values of ISI induced significantly different latencies at the POm and spike counts at the VPM [e.g., 11 Hz with 20 ms (ISI = 71 ms) and 8 Hz with 50 ms (ISI = 75 ms), see relevant data points in Fig. 8]. Regression analysis showed that the ISI can account for 22% of the variability (i.e., $r^2 = 0.22$) in the spike counts of VPM local populations and 28% of the variability in the latencies of POm local populations, while

FIG. 4. *A*: response patterns of all well-localized local populations. All local populations recorded from well-defined recording sites, which were clearly confined to a given nucleus, are included. The steady-state PSTHs for 2, 5, 8, and 11 Hz (color coded as in Fig. 3) are depicted. Firing rate scales were normalized for each local population independently. *B*: examples of single-unit responses. Three single units from each nucleus are depicted. For VPM, Pr5, and Sp5I, the single units belong to the 3 local populations whose responses are depicted in the *top rows* in *A*, from *left* to *right*, respectively. For POm, the 2 leftward single units were recorded from the same electrode (*top left local population* in *A*), and the 3rd single unit belongs to the local population presented *2nd from left* in *A*.
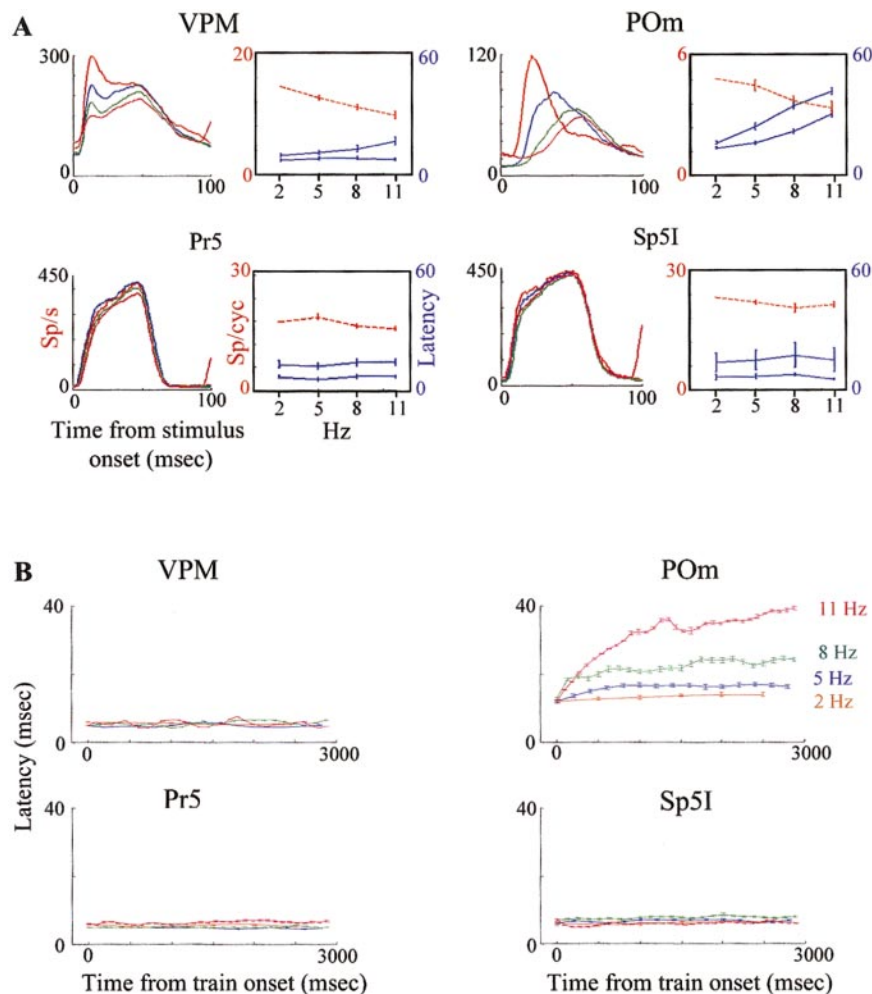
FIG. 6. Neuronal representations of the entire well-localized neuronal ensembles. *A*: steady-state representations. The PSTHs were averaged across all local populations of each nucleus. The latency and spike-count tuning curves were computed for each local population and then averaged. Tuning curves of spike-counts (red dotted curves) were normalized before averaging such that the response of each local population at 2 Hz was equal to the average response of all local populations of that nucleus at 2 Hz. Tuning curves of latency (blue solid curves) were not normalized. Two latency curves are depicted: the *top curve* was computed for a threshold level of 0.5 and the *bottom* for a threshold level of 0.1. Mean ± SE values across all local populations are depicted (SEs represent variability between populations). *B*: dynamics of response latency. For each nucleus and each stimulus frequency, ensemble spike trains were composed of all spikes generated by the different units recorded from the same station in different subjects and at different times. Spike times were aligned according to onset times of the stimulus trains. The latency to 0.3 peak value was computed and plotted for each stimulus cycle. SEs of the latency were computed from the inter-train variability ($n = 24$ trains) of the ensemble latency to the first spike (for each stimulus cycle). Time constants of single-exponential best fits for the latencies of the POm ensemble were: 1,063, 466, 193, and 719 ms for 2, 5, 8, and 11 Hz, respectively. With latencies to 0.1 and 0.5 peak value (not shown) the time constants were: 310, 1,790, 673, 684, and 1,063, 404, 321, and 499, respectively.

the stimulus frequency can account for 50 and 53% of the variability of these variables, respectively, during 50-ms pulse-width stimulations ($P < 0.0001$ for all these regressions).

DISCUSSION

Our findings show that the vibrissal nuclei in the rat thalamus are not simple relays. The neurons of the brain stem trigeminal nuclei closely follow the pattern of stimulation. In contrast, thalamic signals are profoundly transformed. We observed these transformations by investigating neuronal representations of whisking-like stimuli (air-puff stimulations for 50 ms of groups of whiskers in the protraction direction). We focused on transformations in the time and amplitude domains but not in space since the latter domain has already been rigorously investigated (Chiaia et al. 1991b; Diamond et al. 1992; Friedberg et al. 1999; Jacquin et al. 1986; Rhoades et al. 1987; Nicolelis and Chapin 1994; Shipley 1974).

The stimulus frequency was represented by spike counts in both VPM and POm. Nevertheless, these two representations stem from very different transformations involving primarily amplitude reductions in the VPM and primarily latency increments in the POm (Figs. 3–6). Manipulations of the stimulus pulse width revealed another difference: while the spike-count code of the POm was invariant to variations in the stimulus pulse width, that of the VPM was not. The constancy of the spike-count coding in the POm was generated by an adaptive reduction of the latency coding (Fig. 8). This behavior is

consistent with a phase-locked loop operation of paralemniscal thalamocortical loops, which translate vibrissal temporal information, such as the whisker frequency, into a rate code (see *Model of POm operation* below).

Why would the trigeminal system extract information about the frequency of whisker movement from sensory signals while this information is available at the motor system? There are at least two reasons for such sensory processing. The first is that no efference copy of the motor output appears to be relayed to the sensory system (Fee et al. 1997). The second reason is that the sensory generation of the internal representations of the whisker frequency "sets the stage" for the ensuing decoding of sensory information obtained during whisking. For example, part of the information about object location is encoded in the temporal interval between onset of whisker protraction and touching the object (Ahissar and Zacksenhouse 2001). The decoding of this information can be achieved with the same circuits that decode free-air frequency because in both cases the information is encoded in temporal intervals. Thus if the whisking frequency is represented by thalamocortical spike counts, object location will be represented as a deviation from the free-air representation (Ahissar et al. 1997). Furthermore, thalamocortical phase-locked loops can decode object location within a single whisking cycle. However, this is possible only if the sensory system is prelocked to the whisking frequency and the thalamic representations are already stabilized (Ahissar 1998; Ahissar et al. 1997).
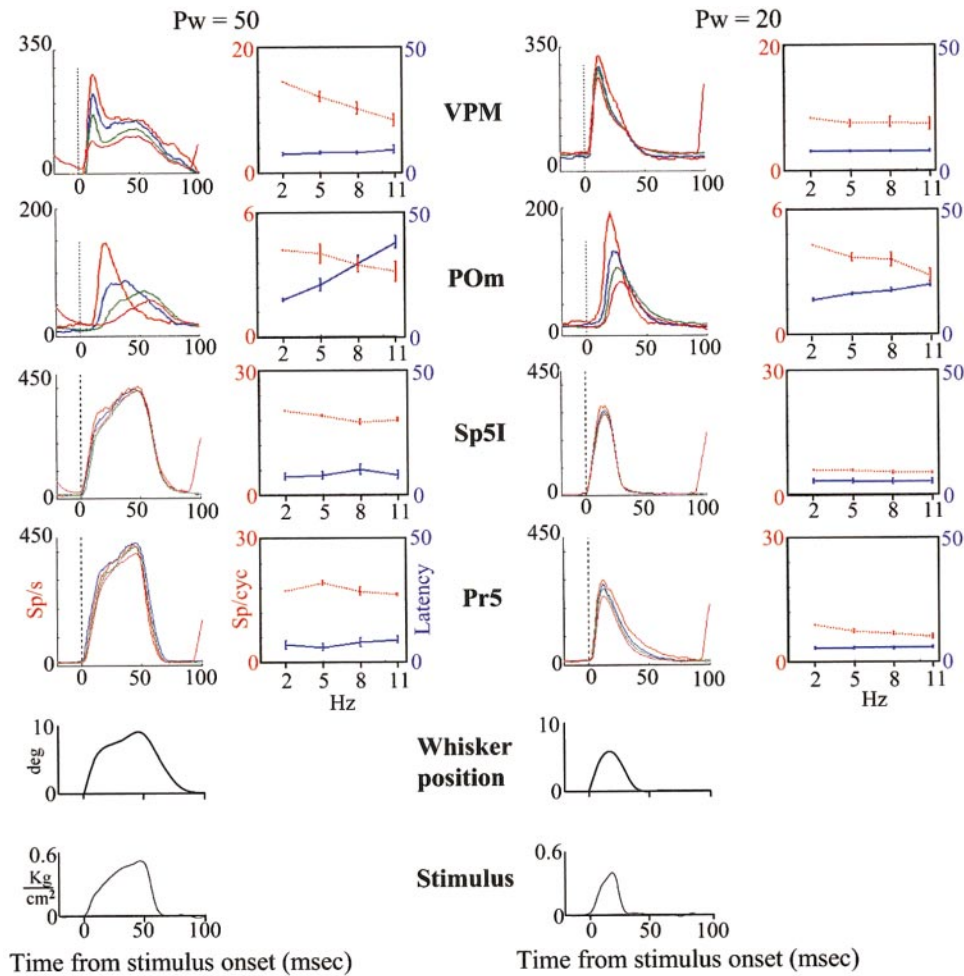
FIG. 7. Effect of the stimulus pulse width on the steady-state responses of neuronal ensembles. For each nucleus and each pulse width, average PSTHs (*left*) and average tuning curves (*right*) are presented. The latency and spike-count tuning curves were computed for each local population and then averaged. Averaging and normalization as in Fig. 6. All well-localized local populations that were stimulated with both 20- and 50-ms pulses were averaged in the VPM ($n = 7$), POm ($n = 8$), and Sp5I ($n = 4$). For Pr5, different local populations were averaged for 20 ($n = 8$) and 50 ms ($n = 6$) pulse widths since only 2 local populations in Pr5 were stimulated with both pulse widths. Whisker position was captured with a motion scope (see legend of Fig. 1).

Effects of anesthesia

VPM neurons showed noticeable amplitude adaptation for 50-ms stimuli (Fig. 6). When stimuli of shorter duration (10 ms) are applied under light anesthesia, no amplitude adaptation is observed in VPM (Hartings and Simons 1998). While anesthesia might have an effect on amplitude adaptation, our findings of almost no amplitude adaptation with 20-ms stimuli (Figs. 8 and 9) suggest that amplitude adaptation is primarily a function of the pulse width and not of the arousal state. The latency shifts observed in the paralemniscal system cannot be attributed to the anesthesia because latency shifts due to anesthesia are an order of magnitude smaller than those observed here (Fanselow and Nicolelis 1999; Friedberg et al. 1999; Simons et al. 1992). Also the observed latency shifts were much smaller for pulse widths of

20 ms than for those of 50 ms under the same conditions of anesthesia. Since latency shifts developed during each stimulus train, they are likely to reflect a dynamic process, specific to processing the sensory stimulus, rather than a general arousal effect. In general, although urethan anesthesia might produce excitatory effects that are not necessarily observed under other anesthetics, or in wakefulness, no frequency-specific effects that could account for our results had been reported so far.

Brain-stem-to-thalamus transformations and thalamic representations

Brain stem neurons, in both Pr5 and Sp5I, usually responded as expected of relay neurons, whose activity directly reflects the sensory transduction stage. Brain stem neurons mainly replicated
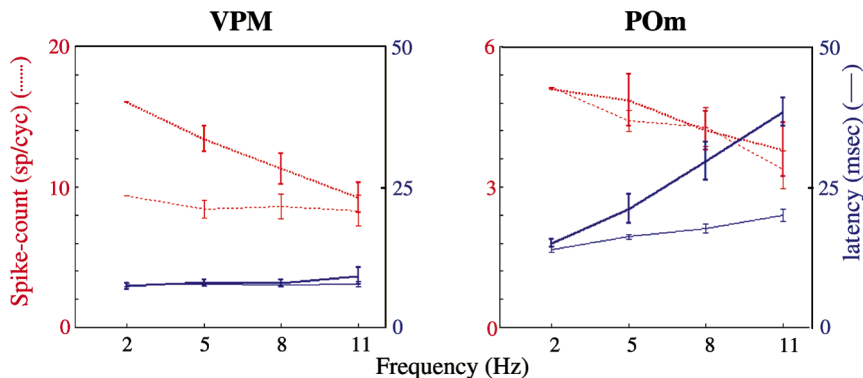

FIG. 8. Dependence of thalamic representations on stimulus frequency and pulse width. Data are re-plotted from Fig. 7. Blue solid curves, latency; red dotted curves, spike-count; thick curves, pulse width of 50 ms; thin curves, pulse width of 20 ms.
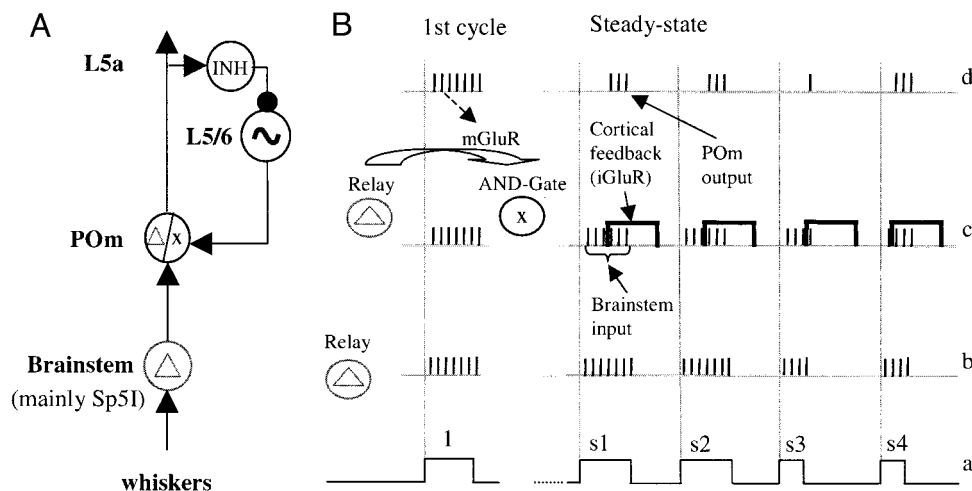
FIG. 9. Paralemniscal thalamocortical model and prediction. *A*: the basic phase-locked loop. POm neurons (Δ/x; Δ, relay mode; x, AND-gate mode) (Sherman and Guillery 1996) drive cortical inhibitory neurons (INH) (Swadlow 1995), which in turn inhibit cortical oscillatory, or intrinsically bursting neurons (Ahissar et al. 1997; Silva et al. 1991; Swadlow 1995), which drive the cortical feedback. Filled circle, inhibitory connection; arrows, excitatory connections (see White and Keller 1987 for an equivalent anatomical circuit). *B*: a timing diagram describing the transition of POm neurons from relay (Δ) to AND-gate (x) mode, and the effect of the stimulus pulse width. Short vertical lines represent spikes. Long vertical lines represent stimulus-pulse onset. Traces: a, whisker deflection, up denotes protraction; b, brain stem response; c, AND-gate operation at the POm: bold rectangles represent the cortical feedback; only those brain stem spikes overlapping with the cortical feedback should "pass the gate"; and d, the output of the POm. Following a quiescent period, POm neurons are hyperpolarized and thus shift into a relay mode (Sherman and Guillery 1996). The response to the 1st stimulus cycle (cycle 1) is relayed to the cortex (activity not shown in the diagram). The cortical feedback activates metabotropic (mGluR) and ionotropic (iGluR) receptors at the thalamus (McCormick and von Krosigk 1992; Salt and Eaton 1996; Sherman and Guillery 1996). The slow mGluR activation depolarizes the thalamic neurons and shift them into an AND-gate mode (Sherman and Guillery 1996), in which brain stem activity will "pass the POm gate" only when additional cortical feedback (via iGluR) is active. When the stimulus pulse width is shortened (cycles s3 and s4), the latency of the cortical feedback should be reduced to keep the output spike count constant.

the temporal pattern of the stimulus; the response amplitude was constant and the duration of the responses followed the stimulus pulse width regardless of the stimulus frequency (Fig. 7). The stimulus frequency is encoded (represented) by the inter-burst intervals of brain stem activity. However, this primary representation must be transformed to other forms in the brain before it can control other functions. For example, if a sensory representation of the whisker frequency is used to control whisker movement within a sensory-motor feedback loop (Kleinfeld et al. 1999), it must be transformed into a rate code since cortical motor commands are encoded primarily by rate (Fetz 1993; Georgopoulos 1986; Kleinfeld et al. 1999; Wise 1993; Zhang and Barash 2000). Similarly, perceptual qualities appear not to be encoded by the temporal patterns that directly replicate the stimulus but by other coding schemes using various rate codes (Salinas et al. 2000; Shadlen and Newsome 1994). Thus the replications of external stimuli, directly reflecting signal transduction, are transformed at subsequent processing stages to more abstract neuronal representations that are more adequate for perception and initiation of movements.

Our results demonstrate that the first transformations into internal coding schemes occur already at the thalamic level. Two different transformations occur in parallel, one resulting in amplitude and spike-count coding in the VPM and another in latency and spike-count coding in the POm. Which of these thalamic representations (amplitude, latency and spike count) is used for further computations by the cortex is not yet known. However, neuronal representations, which are used for further processing, are expected to be protected to some extent from variation in stimulus parameters. Here, the only invariant representation was that of the spike count at the POm. Thus the POm spike count might be the output variable that encodes stimulus frequency for

cortical computations. In that case, the latency coding in the POm may serve as an intermediary to obtain the spike-count coding and as such would indeed be changed along with the change in the stimulus pulse width to keep the output spike count unchanged (see *Model of POm operation* below). The inconsistency of the VPM spike-count coding suggests that this representation is not a "true" representation of the stimulus temporal frequency but rather a byproduct of a different process, possibly one that performs a rate-coded spatial computation.

Here spike counts were the entire counts of spikes within the response window rather than the counts beyond those expected by spontaneous firing, a measure that is often used to estimate neuronal responses. Although the difference between the two measures was small, we used the former measure to be able to interpret our results in terms of neuronal representations that underlie further neuronal processing; obviously, what a neuronal station that processes these neuronal representations (a "readout" station) receives as an input is the total count of spikes and not the differential one. Similarly, the latency of the input to the readout station is determined by the entire response and thus latency to first spike should be more appropriate. Unfortunately, latency to first spike is strongly affected by cell excitability (see METHODS and following text) and thus cannot be used to estimate latencies independently from spike counts. Here, since spontaneous and tonic activities were usually much lower than evoked ones, latencies estimated from the rising edge of the PSTH provided good estimation of activation times. Moreover, the rising edges of PSTHs are good predictors of activation times at the read-out stations (compare brain stem responses with those of thalamic neurons here and of cortical neurons in the accompanying paper, Ahissar et al. 2001).

Comparison of present with previous findings

BRAIN STEM. The activity of Pr5 and Sp5I local populations followed the movement pattern of the stimulated whiskers for all tested frequencies (Figs. 1, 2, 4, 6, and 8). This response pattern is consistent with previous recordings from the rat trigeminal nuclei. By recording from the anterior part of the trigeminal complex of the brain stem, Shipley (1974) identified three types of responsive neurons: tonic, phasic-summators, and phasic-velocity. The tonic cells were restricted to the most anterior part of the complex, probably Pr5, whereas the phasic neurons were distributed across the entire recording area, probably Pr5 and Sp5O. Shipley observed that both tonic and phasic-summator cells, which together composed almost 80% of the sample, fire tonically as long as the whiskers are moving, and that the spike counts that are generated by these cells are proportional to the deflection amplitude. Since our air-puff stimulations induced continuous whisker movements (Fig. 1), the responses of these two cell types are expected to be similar to the population responses presented here in response to our air-puff stimulations. Tonic population responses were also observed in Pr5 and Sp5 during the protraction phase of self-initiated whisker movements (Nicolelis et al. 1995), movements whose pattern should not be much different from the pattern induced by our air puffs [compare the whisker trajectory depicted in our Fig. 1 with those of single whisking cycles described in Fig. 4 of Carvell and Simons (1990)]. Shipley (1974) also noticed that the response pattern depends on the stimulus velocity: higher velocities usually yielded more phasic responses. Our results are consistent with this observation as well. In our study, the same neurons exhibited tonic responses to air-puff stimuli, and phasic or phasic/tonic responses to mechanical stimuli, with the mechanical stimuli eliciting faster vibrissal deflections than the air-puff ones (see Fig. 1).

THALAMUS. In a pioneering study, Diamond and colleagues demonstrated the following basic differences between the responses of VPM and POm single units in anesthetized rats to brief (3 ms) mechanical stimulations of single whiskers (Diamond et al. 1992). VPM spike counts are constant between 0.2 and 5 Hz and start to decrease between 5 and 10 Hz [in lightly narcotized rats, VPM responses to short pulses are constant up to $\geq$12 Hz (Hartings and Simons 1998)]. In contrast, POm spike counts decrease monotonically between 1 and 10 Hz (Diamond et al. 1992). The findings of our study are consistent with their results: with short pulse widths, VPM spike counts were almost constant, whereas POm spike counts decreased monotonically between 2 and 11 Hz (Figs. 8 and 9). Although Diamond et al. observed that POm neurons display latency increments at frequencies >1 Hz, these dynamics were not quantified perhaps because of the weak POm responsiveness to single-whisker stimulations. The majority of POm neurons respond much stronger to multi-whisker stimuli (Diamond et al. 1992), such as those that occur during natural whisking. In our study, multi-whisker stimulations and analysis of local populations provided sufficient data for quantitative analysis, which demonstrated robust latency coding in the POm. Although latency shifts were not quantified by Diamond et al. (1992), their data indicate that the temporal modulations were not as large as with the 50-ms air-puff pulses used here but rather were closer to the smaller latency shifts observed here with 20-ms air-puff pulses (Fig. 7). Overall, the data of Dia-

mond et al. and our data are consistent with the extent of latency modulations in the POm being dependent on the duration of the tonic activation of brain stem neurons. During the protraction period of natural whisking, the whiskers of rats move continuously for 50 ms (Carvell and Simons 1990), and most brain stem neurons respond tonically to continuous movements (Figs. 1, 2 and 4) (see also Nicolelis et al. 1995; Shipley 1974), therefore the brain stem bursts that were observed here with 50-ms air-puff pulses should be similar to the shortest brain stem trains produced during whisking (note that protraction cycles are usually >50 ms, Carvell and Simons 1990). Thus the range of POm latency modulations observed here is probably the lower limit of the ranges of latency modulations that occur during natural whisking.

ESTIMATION OF RESPONSE LATENCY. Despite their long steady-state latencies, the onset activation of POm populations, following a quiescent period, is only 1–2 ms later than that of the VPM (Ahissar et al. 2000). This result is consistent with the 1- to 2-ms delay between VPM and POm responses to brain stem electrical stimulations (Chiaia et al. 1991b). Nevertheless, it seems to contradict a previously reported delay of 8–16 ms between VPM and POm latencies (Diamond et al. 1992). This apparent contradiction may be due to the methods used to calculate response latency. Whereas we used latency to the rising edge of the firing probability (described by the PSTH), Diamond et al. (1992) used latency to the first spike after stimulus onset. A drawback of the latter method is that the latency to the first spike is strongly related to the firing probability; typically, lower probabilities yield longer delays to the first spike. Consider, for example, two PSTHs that have the same shape except that one has a larger amplitude. Although both PSTHs begin to rise at the same latency and reach their maximal firing probability at the same latency, the probability of finding the first spike earlier in every given trial is higher for the unit with the higher firing rate. Since single units in the POm respond with lower firing rates than VPM neurons, the comparison of latencies to first spikes is biased toward longer latencies of POm neurons. While latency to first spike is probably relevant for most neuronal computations (see text in previous section), it cannot serve as a basis for the estimation of the order or the delay of activation between different neuronal populations.

The definition of response latency is not unique. In fact, a practical definition of response latency should be based on the operation and sensitivity of the relevant readout circuit that processes the neuronal activity under investigation. Since here the computations done by the relevant readout circuits are not known, we used a straight-forward estimation of the latency to the onset of poststimulus activation that is the least affected by the peculiarities of our stimulation protocol and by absolute changes in firing rates (see METHODS). This threshold-crossing estimation was usually reliable for determining activation onsets as judged by visual inspections of rasters and PSTHs. Together with the spike-count measure, this latency estimation captured the main transformations that occurred at the thalamus except that of the change in the balance between early and late response components in the VPM as a function of the frequency. This effect, whose cause or function are not yet clear, is evident in the PSTHs of many VPM recordings (Fig. 4).

Air-puff versus mechanical stimuli

Air-puff stimuli force whiskers only in one direction (protraction in this study), while movement in the other direction is passive, thus mimicking natural whisking (Kleinfeld et al. 1999). Indeed, these air-puff stimuli cause an activation pattern in the brain stem of anesthetized rats (e.g., Fig. 6*A*) that is similar to the pattern observed in the freely moving rat (Nicolelis et al. 1995); brain stem neurons respond only to the whisker protraction, not the retraction (Fig. 1). In contrast, mechanical stimulations, which force whisker movement in both directions, usually evoke ON and OFF phasic responses (Fig. 1), which probably do not occur during natural whisking. These responses are probably primarily affected by the high-frequency components contained in the fast transitions usually characterizing mechanical stimuli. Thus our data suggest that for mimicking the conditions of whisking, unidirectional slow stimulations are preferable. Of course, for simulating touch during whisking, mechanical obstacles or stimulators are appropriate.

Model of POm operation

Gating of POm responses (Figs. 3–6), and the dynamics of stabilization (Figs. 2, 3*B,* and 6*B*) observed here are consistent with the PLL model of temporal- to rate-code transformation by thalamocortical loops (Ahissar 1998; Ahissar and Vaadia 1990; Ahissar et al. 1997, 2000). According to this model, POm neurons are gated by the output of cortical oscillatory neurons, that are inhibited by the output of POm neurons, via cortical inhibitory neurons (Fig. 9*A*).

Thalamocortical neurons possess two modes of operation, "relay" and "gate" (McCormick and von Krosigk 1992; Sherman and Guillery 1996). Following a quiescent period, thalamic neurons are shifted to a hyperpolarized sensitive mode, in which their output does not appear to depend on the cortical signal (a relay mode). This can explain the relatively short latency of POm neurons to the first stimulus cycle (Figs. 1–3) and the relatively long period required for stabilization (Fig. 6*B*). During on-going stimulations, thalamocortical neurons are continuously depolarized, probably via cortically controlled metabotropic glutamate receptors (mGluRs) (McCormick and von Krosigk 1992; Salt and Eaton 1996), and are assumed to function in an "AND-gate" mode (Sherman and Guillery 1996). In this mode, POm neurons should be active only when their two major inputs, from the brain stem and cortex (via ionotropic glutamate receptors, iGluRs), are co-active. Within each stimulus cycle (Fig. 9*B*), the onset latency of this co-activation is the onset latency of the cortical feedback within that cycle (Fig. 9*B*, bold rectangles) since the cortical feedback lags the brain stem onset. In contrast, the offset latency of the co-activation is the offset latency of the brain stem since brain stem offset leads the offset of the cortical feedback. Since the offset latency of brain stem activity is constant (for a given pulse width; Figs. 4, 6, and 7), the offset latency of the POm should also be constant, just as we observed here. In contrast, the onset latency of the POm should vary with the onset latency of cortical oscillating neurons (Ahissar et al. 1997).

Can this model explain the observed dependence of POm latency and spike count on the frequency (Fig. 6*A*)? According to this model, the modulation in spike counts as a function of input frequency results from the modulation of the latency of the cortical oscillatory neurons. On the other hand, the POm spike count controls the frequency of the cortical oscillatory neurons via inhibition. Thus both latency and spike count should change with the frequency. Since the frequency of cortical oscillatory neurons increases with increased local excitation (Ahissar et al. 1997; Silva et al. 1991), the directions of changes should be, according to the model, as follows. POm spike count must decrease (to reduce the inhibition), and thus the latency must increase (to reduce the spike count), with increasing stimulus frequencies, as long as the thalamocortical loop (including the cortical oscillating neurons) follows the input frequency. This is exactly what we observed (Fig. 6*A*). Thus for each stimulus frequency, there exists a pair of values that defines the loop set-point for that frequency; the POm spike count, which is determined by the frequency, and the POm latency, which is determined by the spike count. This provides the following prediction: when the dependency (i.e., transfer function) between the POm spike count and latency changes, the spike count should preserve its frequency dependence (since it is directly related to the cortical oscillating frequency) while the latency should be adjusted.

This prediction was tested by our pulse-width experiment. Shortening the air-puff pulses to 20 ms shortened the duration of the brain stem outputs by a similar amount (Fig. 7). Such a shortening should change the transfer function between latency and spike count in the POm (Fig. 9*B*, stimulus cycles s3, s4): latencies that generate a number of spikes with long stimulus pulses (3 spikes in the example depicted in Fig. 9), generate less spikes (1 in the example, cycle s4) with shorter pulses. If the spike count has to be preserved, latencies should be shortened (Fig. 9*B*, cycle s4). Indeed, this is what we observed in the POm (and in its main output station, layer 5a of the barrel cortex, Ahissar et al. 2001): while the spike-count code was preserved, the latencies were significantly shortened (Figs. 7 and 8). It is remained to see whether this shortening is indeed due to a similar shortening in the delay of cortical oscillators, as predicted by the PLL model.

REFERENCES

ABELES M. A journey into the brain. In: *Signal Analysis and Pattern Recognition in Biomedical Engineering,* edited by Inbar GF. New York: Wiley, 1975, p. 41–59.

ABELES M. *Local Cortical Circuits: An Electrophysiological Study.* Berlin: Springer, 1982.

AHISSAR E. Temporal-code to rate-code conversion by neuronal phase-locked loops. *Neural Comput* 10: 597–650, 1998.

AHISSAR E, HAIDARLIU S, AND ZACKSENHOUSE M. Decoding temporally encoded sensory input by cortical oscillations and thalamic phase comparators. *Proc Natl Acad Sci USA* 94: 11633–11638, 1997.

AHISSAR E, SOSNIK R, BAGDASARIAN K, AND HAIDARLIU S. Temporal frequency of whisker movement. II. Laminar organization of cortical representations. *J Neurophysiol* 86: 354–367, 2001.

AHISSAR E, SOSNIK R, AND HAIDARLIU S. Transformation from temporal to rate coding in a somatosensory thalamocortical pathway. *Nature* 406: 302–306, 2000.

AHISSAR E AND VAADIA E. Oscillatory activity of single units in a somatosensory cortex of an awake monkey and their possible role in texture analysis. *Proc Natl Acad Sci USA* 87: 8935–8939, 1990.

AHISSAR E AND ZACKSENHOUSE M. Temporal and spatial coding in the rat vibrissal system. *Prog Brain Res* 130: 75–88, 2001.

ARMSTRONG-JAMES M AND CALLAHAN CA. Thalamo-cortical processing of vibrissal information in the rat. II. Spatiotemporal convergence in the thalamic ventroposterior medial nucleus (VPm) and its relevance to generation of receptive fields of S1 cortical "barrel" neurones. *J Comp Neurol* 303: 211–224, 1991.

ARMSTRONG-JAMES M AND FOX K. Spatiotemporal convergence and divergence in the rat S1 "barrel" cortex. *J Comp Neurol* 263: 265–281, 1987.

BISHOP GH. The relation between nerve fiber size and sensory modality: phylogenetic implications of the afferent innervation of cortex. *J Nerv Ment Dis* 128: 89–114, 1959.

BRUCE LL, MCHAFFIE JG, AND STEIN BE. The organization of trigeminotectal and trigeminothalamic neurons in rodents: a double-labeling study with fluorescent dyes. *J Comp Neurol* 262: 315–330, 1987.

CARVELL GE AND SIMONS DJ. Biometric analyses of vibrissal tactile discrimination in the rat. *J Neurosci* 10: 2638–2648, 1990.

CHIAIA NL, RHOADES RW, BENNETT-CLARKE CA, FISH SE, AND KILLACKEY HP. Thalamic processing of vibrissal information in the rat. I. Afferent input to the medial ventral posterior and posterior nuclei. *J Comp Neurol* 314: 201–216, 1991a.

CHIAIA NL, RHOADES RW, FISH SE, AND KILLACKEY HP. Thalamic processing of vibrissal information in the rat. II. Morphological and functional properties of medial ventral posterior nucleus and posterior nucleus neurons. *J Comp Neurol* 314: 217–236, 1991b.

DIAMOND ME. Somatosensory thalamus of the rat. *Cereb Cortex* 11: 189–219, 1995.

DIAMOND ME AND ARMSTRONG-JAMES M. Role of parallel sensory pathways and cortical columns in learning. *Concepts Neurosci* 3: 55–78, 1992.

DIAMOND ME, ARMSTRONG-JAMES M, AND EBNER FF. Somatic sensory responses in the rostral sector of the posterior group (POm) and in the ventral posterior medial nucleus (VPM) of the rat thalamus. *J Comp Neurol* 318: 462–476, 1992.

ERZURUMLU RS AND KILLACKEY HP. Diencephalic projections of the subnucleus interpolaris of the brainstem trigeminal complex in the rat. *Neuroscience* 5: 1891–1901, 1980.

FANSELOW EE AND NICOLELIS MAL. Behavioral modulation of tactile responses in the rat somatosensory system. *J Neurosci* 19: 7603–7616, 1999.

FEE MS, MITRA PP, AND KLEINFELD D. Central versus peripheral determinants of patterned spike activity in rat vibrissa cortex during whisking. *J Neurophysiol* 78: 1144–1149, 1997.

FETZ EE. Cortical mechanisms controlling limb movement. *Curr Opin Neurobiol* 3: 932–939, 1993.

FRIEDBERG MH, LEE SM, AND EBNER FF. Modulation of receptive field properties of thalamic somatosensory neurons by the depth of anesthesia. *J Neurophysiol* 81: 2243–2252, 1999.

GEORGOPOULOS AP. On reaching. *Annu Rev Neurosci* 9: 147–170, 1986.

GEORGOPOULOS AP, TAIRA M, AND LUKASHIN A. Cognitive neurophysiology of the motor cortex. *Science* 260: 47–52, 1993.

GHAZANFAR AA AND NICOLELIS MA. Nonlinear processing of tactile information in the thalamocortical loop. *J Neurophysiol* 78: 506–510, 1997.

GHAZANFAR AA, STAMBAUGH CR, AND NICOLELIS MA. Encoding of tactile stimulus location by somatosensory thalamocortical ensembles. *J Neurosci* 20: 3761–3775, 2000.

HAIDARLIU S. An anatomically adapted, injury-free headholder for guinea pigs. *Physiol Behav* 60: 111–114, 1996.

HAIDARLIU S AND AHISSAR E. Spatial organization of facial vibrissae and cortical barrels in the guinea pig and golden hamster. *J Comp Neurol* 385: 515–527, 1997.

HAIDARLIU S AND AHISSAR E. Size gradients of barreloids in the rat thalamus. *J Comp Neurol* 429: 372–387, 2001.

HAIDARLIU S, SHULZ D, AND AHISSAR E. A multielectrode array for combined microiontophoresis and multiple single-unit recordings. *J Neurosci Methods* 56: 125–131, 1995.

HAIDARLIU S, SOSNIK R, AND AHISSAR E. Simultaneous multi-site recordings and iontophoretic drug and dye applications along the trigeminal system of anesthetized rats. *J Neurosci Methods* 94: 27–40, 1999.

HARTINGS JA AND SIMONS DJ. Thalamic relay of afferent responses to 1- to 12-Hz whisker stimulation in the rat. *J Neurophysiol* 80: 1016–1019, 1998.

JACQUIN MF, MOONEY RD, AND RHOADES RW. Morphology, response properties, and collateral projections of trigeminothalamic neurons in brainstem subnucleus interpolaris of rat. *Exp Brain Res* 61: 457–468, 1986.

KLEINFELD D, BERG RW, AND O'CONNOR SM. Anatomical loops and their electrical dynamics in relation to whisking by rat. *Somatosens Mot Res* 16: 69–88, 1999.

MCCORMICK DA AND VON KROSIGK M. Corticothalamic activation modulates thalamic firing through glutamate "metabotropic" receptors. *Proc Natl Acad Sci USA* 89: 2774–2778, 1992.

NICOLELIS MA AND CHAPIN JK. Spatiotemporal structure of somatosensory responses of many-neuron ensembles in the rat ventral posterior medial nucleus of the thalamus. *J Neurosci* 14: 3511–3532, 1994.

NICOLELIS MAL, BACCALA LA, LIN RCS, AND CHAPIN JK. Sensorimotor encoding by synchronous neural ensemble activity at multiple levels of the somatosensory system. *Science* 268: 1353–1358, 1995.

NICOLELIS MAL, LIN RCS, WOODWARD DJ, AND CHAPIN JK. Dynamic and distributed properties of many-neuron ensembles in the ventral posterior medial thalamus of awake rats. *Proc Natl Acad Sci USA* 90: 2212–2216, 1993.

PESCHANSKI M. Trigeminal afferents to the diencephalon in the rat. *Neuroscience* 12: 465–487, 1984.

PETERSEN RS AND DIAMOND ME. Spatial-temporal distribution of whisker-evoked activity in rat somatosensory cortex and the coding of stimulus location. *J Neurosci* 20: 6135–6143, 2000.

RAIGUEL SE, XIAO DK, MARCAR VL, AND ORBAN GA. Response latency of macaque area MT/V5 neurons and its relationship to stimulus parameters. *J Neurophysiol* 82: 1944–1956, 1999.

RHOADES RW, BELFORD GR, AND KILLACKEY HP. Receptive-field properties of rat ventral posterior medial neurons before and after selective kainic acid lesions of the trigeminal brain stem complex. *J Neurophysiol* 57: 1577–1600, 1987.

SALINAS E, HERNANDEZ A, ZAINOS A, AND ROMO R. Periodicity and firing rate as candidate neural codes for the frequency of vibrotactile stimuli. *J Neurosci* 20: 5503–5515, 2000.

SALT TE AND EATON SA. Functions of ionotropic and metabotropic glutamate receptors in sensory transmission in the mammalian thalamus. *Prog Neurobiol* 48: 55–72, 1996.

SCHNEIDER W. The tactile array stimulator. *Johns Hopkins APL Technical Digest* 9: 39–43, 1988.

SHADLEN MN AND NEWSOME WT. Noise, neural codes and cortical organization. *Curr Opin Neurobiol* 4: 569–579, 1994.

SHERMAN SM AND GUILLERY RW. Functional organization of thalamocortical relays. *J Neurophysiol* 76: 1367–1395, 1996.

SHIPLEY MT. Response characteristics of single units in the rat's trigeminal nuclei to vibrissa displacements. *J Neurophysiol* 37: 73–90, 1974.

SILVA LR, AMITAI Y, AND CONNORS BW. Intrinsic oscillations of neocortex generated by layer 5 pyramidal neurons. *Science* 251: 432–435, 1991.

SIMONS DJ. Neuronal integration in the somatosensory whisker/barrel cortex. *Cereb Cortex* 11: 263–297, 1995.

SIMONS DJ AND CARVELL GE. Thalamocortical response transformation in the rat vibrissa/barrel system. *J Neurophysiol* 61: 311–330, 1989.

SIMONS DJ, CARVELL GE, HERSHEY AE, AND BRYANT DP. Responses of barrel cortex neurons in awake rats and effects of urethane anesthesia. *Exp Brain Res* 91: 259–272, 1992.

SWADLOW HA. Influence of VPM afferents on putative inhibitory interneurons in S1 of the awake rabbit: evidence from cross-correlation, microstimulation, and latencies to peripheral sensory stimulation. *J Neurophysiol* 73: 1584–1599, 1995.

VEINANTE P, JACQUIN MF, AND DESCHENES M. Thalamic projections from the whisker-sensitive regions of the spinal trigeminal complex in the rat. *J Comp Neurol* 420: 233–243, 2000.

WAITE PM. The responses of cells in the rat thalamus to mechanical movements of the whiskers. *J Physiol (Lond)* 228: 541–561, 1973.

WELKER WI. Analysis of sniffing of the albino rat. *Behaviour* 22: 223–244, 1964.

WHITE EL AND KELLER A. Intrinsic circuitry involving the local axon collaterals of corticothalamic projection cells in mouse SmI cortex. *J Comp Neurol* 262: 13–26, 1987.

WILLIAMS MN, ZAHM DS, AND JACQUIN MF. Differential foci and synaptic organization of the principal and spinal trigeminal projections to the thalamus in the rat. *Eur J Neurosci* 6: 429–453, 1994.

WISE SP. Monkey motor cortex: movements, muscles, motoneurons and metrics. *Trends Neurosci* 16: 46–49, 1993.

WOOLSEY TA. Barrels, vibrissae and topographic representations. In: *Encyclopedia of Neuroscience,* edited by Adelman G and Smith B. Amsterdam: Elsevier, 1997, vol. I, p. 195–199.

ZHANG M AND BARASH S. Neuronal switching of sensorimotor transformations for antisaccades. *Nature* 408: 971–975, 2000.